View metadata, citation and similar papers at core.ac.uk

brought to you by CORE

provided by University of Dayton

University of Dayton
eCommons

Chemical and Materials Engineering Faculty Publications

Department of Chemical and Materials Engineering

2014

# Continuous Ultra-Thin MoS2 Films Grown by Low-Temperature Physical Vapor Deposition

Christopher Muratore
*University of Dayton*, cmuratore1@udayton.edu

Jianjun Hu
*University of Dayton*, jhu001@udayton.edu

Baoming Wang
*Pennsylvania State University - Main Campus*

M. Amanul Haque
*Pennsylvania State University - Main Campus*

John E. Bultman
*University of Dayton*, jbultman1@udayton.edu

***See next page for additional authors***

Follow this and additional works at: https://ecommons.udayton.edu/cme_fac_pub


Part of the Other Chemical Engineering Commons, Other Materials Science and Engineering Commons, and the Polymer and Organic Materials Commons

eCommons Citation

Muratore, Christopher; Hu, Jianjun; Wang, Baoming; Haque, M. Amanul; Bultman, John E.; Jespersen, Michael L.; McConney, Michael E.; and Naguy, R. D., "Continuous Ultra-Thin MoS2 Films Grown by Low-Temperature Physical Vapor Deposition" (2014). *Chemical and Materials Engineering Faculty Publications*. 99.
https://ecommons.udayton.edu/cme_fac_pub/99

This Article is brought to you for free and open access by the Department of Chemical and Materials Engineering at eCommons. It has been accepted for inclusion in Chemical and Materials Engineering Faculty Publications by an authorized administrator of eCommons. For more information, please contact frice1@udayton.edu, mschlangen1@udayton.edu.

**Author(s)**
Christopher Muratore, Jianjun Hu, Baoming Wang, M. Amanul Haque, John E. Bultman, Michael L. Jespersen, Michael E. McConney, and R. D. Naguy

This article is available at eCommons: https://ecommons.udayton.edu/cme_fac_pub/99

# Continuous ultra-thin $MoS_2$ films grown by low-temperature physical vapor deposition

C. Muratore,[1,2] J. J. Hu,[2,3] B. Wang,[4] M. A. Haque,[4] J. E. Bultman,[2,3] M. L. Jespersen,[2,3] P. J. Shamberger,[2] M. E. McConney,[2] R. D. Naguy,[2] and A. A. Voevodin[2]
[1]*Department of Chemical and Materials Engineering, University of Dayton, Dayton, Ohio 45469, USA*
[2]*Materials and Manufacturing Directorate, Air Force Research Laboratory, Wright-Patterson AFB, Ohio 45433, USA*
[3]*University of Dayton Research Institute, Dayton, Ohio 45469, USA*
[4]*Department of Mechanical and Nuclear Engineering, Pennsylvania State University, College Park, Pennsylvania 16802, USA*

(Received 3 April 2014; accepted 15 June 2014; published online 1 July 2014)

Uniform growth of pristine two dimensional (2D) materials over large areas at lower temperatures without sacrifice of their unique physical properties is a critical pre-requisite for seamless integration of next-generation van der Waals heterostructures into functional devices. This Letter describes a vapor phase growth technique for precisely controlled synthesis of continuous, uniform molecular layers of $MoS_2$ on silicon dioxide and highly oriented pyrolitic graphite substrates of over several square centimeters at 350 °C. Synthesis of few-layer $MoS_2$ in this ultra-high vacuum physical vapor deposition process yields materials with key optical and electronic properties identical to exfoliated layers. The films are composed of nano-scale domains with strong chemical binding between domain boundaries, allowing lift-off from the substrate and electronic transport measurements from contacts with separation on the order of centimeters. © *2014 AIP Publishing LLC*.
[http://dx.doi.org/10.1063/1.4885391]

Molybdenum disulfide is a naturally abundant material with a layered atomic structure giving rise to remarkable mechanical (e.g., low shear strength for solid lubrication)[1] and catalytic (e.g., hydrodesulfidization)[2] performance. Few-layer $MoS_2$ and other transition metal dichalcogenides (TMDs) have recently shown exciting technological potential in nano-electronic device development such as a thickness-[3] or strain-tunable[4] direct band gap[5,6] enhanced photoluminescence[7] with sensitivity to ambient environments,[8] and other properties with promise for diverse sensor[8,9] and optoelectronic device applications.[10] The thin TMD materials examined in the aforementioned studies have been synthesized primarily by chemical or mechanical exfoliation—both approaches generally lacking scalability and uniformity over appreciable areas ($>10\,\mu$m). Chemical vapor deposition is emerging as a technique to produce continuous transition metal dichalcogenide films, over larger areas ($>10\,\mu m^2$) approaching those of exfoliated crystals;[11] however, the lack of pristine quality, wafer-scale synthesis of continuous two dimensional (2D) TMDs, and their heterostructures is currently a major hurdle impeding both fundamental understanding and device development progress.

Here, results from few-layer $MoS_2$ growth under non-equilibrium physical vapor deposition (PVD) growth of continuous $MoS_2$ films of 3–6 molecular layers at a growth temperature of 350 °C are shown. This is accomplished by maximizing atomic mobility during growth through the use of incident atoms with kinetic energies just below the lowest energy threshold for defect formation (i.e., vacancy creation by sputtering of S atoms), which is reported to be approximately 8 eV.[12] The materials were grown on amorphous $SiO_2$ and (002) oriented graphite substrates in an ultra-high vacuum environment to minimize surface and interface contamination. Examination of the materials via transmission electron microscopy (TEM) and atomic force microscopy (AFM) revealed that they were continuous and of uniform thickness with well-aligned basal planes over 4 $cm^2$ areas. Materials grown via this PVD technique possess characteristics typical of few-layer $MoS_2$ films produced by exfoliation, including an equivalent dependence of Raman peak shifts on thickness[5] and a direct band gap of approximately 1.9 eV.[13]

The PVD synthesis process is based on magnetron sputtering, and is, therefore, easily scalable to allow growth of very thin TMD films over very large areas ($>1$ $m^2$) on diverse substrate materials due to the low processing temperatures. PVD possesses additional advantages in the cleanliness of the interfaces processed in the ultra-high vacuum environment (base pressure was $<5\times10^{-9}$ Torr for all growth experiments) and the precise atomic scale thickness control for well-defined interfaces. This work is an extension of the authors' prior efforts examining PVD process parameters and growth orientation control of nano-crystalline $MoS_2$ films,[14,15] but with emphasis on low temperature growth and large-scale synthesis of few-layer $MoS_2$. All films were grown via magnetron sputtering using a solid 3.3 cm diameter $MoS_2$ target of 99.95% purity. The $SiO_2$ and highly oriented pyrolitic graphite (HOPG) substrates were introduced via a vacuum load-lock and mounted on an electrically grounded, heatable, and rotatable fixture. Square Si substrates with a 1000 nm thermally grown $SiO_2$ with dimensions of 2 cm × 2 cm were ultrasonically cleaned in a series of solvents and rinsed with deionized water. HOPG samples 1 cm × 1 cm (SPI, Grade 1) were mechanically cleaved immediately prior insertion into a sample vacuum load-lock. In this work, the samples were heated to 350 °C and allowed to rotate at approximately 100 rotations per minute while

 © 2014 AIP Publishing LLC

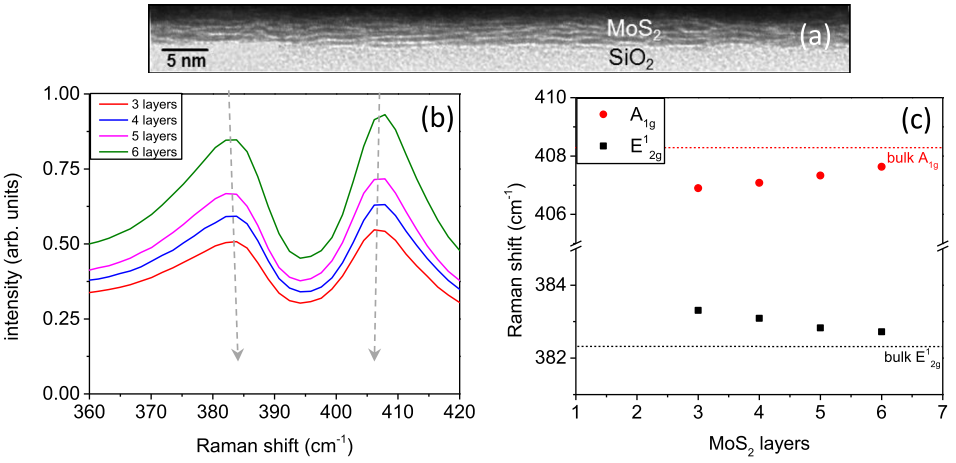


FIG. 1. Typical cross-sectional microstructure of $MoS_2$ films synthesized at 350 °C is shown for a five layer sample on $SiO_2$ in (a). The Raman spectra of films for a range of thicknesses are shown in (b). The frequency shift between in-plane and out-of-plane Raman peaks is correlated to the number of layers (c) by measurement of film thickness in the TEM.

positioned 7 cm from the $MoS_2$ target. Throughout the process, the temperature was measured with an IR pyrometer calibrated with a thermocouple for each substrate material. The chamber was then filled with ultra-high purity argon gas at a constant flow rate of 25 sccm to a pressure of 15 mTorr (2 Pa). Conditions for controlling the orientation of $MoS_2$ films in similar vapor phase growth processes were outlined by the authors in prior works,[14,16] but employing additional control over the desorption and diffusion kinetics of $MoS_2$ by modulating the power to the sputter source and also by controlling the magnetic and electrostatic fields adjacent to the substrate were necessary in the present work. Films were grown layer by layer over incrementally longer time intervals at a constant rate of approximately 0.15 nm per second in order to precisely build their thickness to the desired number of layers. Raman spectroscopy was then employed to characterize $E_{2g}{}^1$ (in-plane vibrations) and $A_{1g}$ (out-of-plane vibrations) peaks indicating atomic ordering into crystalline hexagonal $MoS_2$. The growth time on $SiO_2$ was correlated to the resulting thickness by examining cross sections of several samples grown for different durations in the TEM to precisely identify the number of molecular layers. Samples were prepared for study in the TEM by evaporating a layer of gold onto the surface to protect the $MoS_2$ layers from damage during focused ion beam processing. A typical film cross-section on a thermally grown silicon oxide wafer ($R_a = 5$ nm) is shown in Fig. 1(a) for a five layer thick sample. The atomic layers are parallel with spacings measured to be 0.63–0.68 nm (close to accepted spacing for bulk crystal of 0.66 nm); however, atomic scale boundaries isolate individual crystalline domains with characteristic lengths on the order of 5–10 nm. Despite the nanoscale size of the domains, the materials are apparently bonded through the domain boundaries because large areas (>$mm^2$) of intact films can be lifted off the substrates via solution-based techniques. Additionally, four indium contacts were placed at the corners of an approximately $1 \times 1\ cm^2$ in a van der Pauw geometry on films 3–6 layers thick to measure room-temperature resistance values of $1–5 \times 10^{-4}\ \Omega$-m.

Examples of Raman spectra (514 nm excitation wavelength) for samples grown at different times are shown in Fig. 1(b). The difference between the $E_{2g}{}^1$ and $A_{1g}$ peak shifts (measured by fitting of a Gaussian function to each Raman peak) are plotted against film thickness, as shown in Figure 1(c). Raman spectroscopy has been used to generate topographical surface maps allowing characterization of the number of $MoS_2$ layers and thickness uniformity.[17,18] In these works, the contrast in such maps spatially resolves the frequency difference between $A_{1g}$ and $E_{2g}{}^1$ peaks in the Raman spectra, revealing the number of layers at a particular region of a sample. This mapping technique is effective, but not practical over the $cm^2$ length scale of interest in this work; therefore, a modified Raman technique was developed to evaluate uniformity over large areas. The Raman peak separations for samples of the thickness measured by observation in the TEM were plotted to make a calibration curve relating $A_{1g}$ and $E_{2g}{}^1$ peak separations to the number of layers as shown in Fig.1(c). The peak separations were consistent with those reported in the literature for exfoliated films of the same thickness.[17] Physical vapor deposition (Fig. 2(a)) was used to grow a four-layer $MoS_2$ sample on an oxidized silicon wafer with an area of 4 $cm^2$ (Figure 2(b)) under identical processing conditions as those used to generate the calibration curve (Fig. 2(c)). Raman spectra were collected over the sample area in 500 $\mu$m intervals along the sample length and width. The frequency difference between the $E_{2g}{}^1$ and $A_{1g}$ peaks was measured at the approximate positions identified on the sample as shown in Fig. 2(b). The minimum (24.1 $cm^{-1}$) and maximum (24.3 $cm^{-1}$) frequency values were obtained over the 4 $cm^2$ area shown in Fig. 2(b), indicating the minimum and maximum thicknesses, respectively, on the sample surface. These values are plotted on the $MoS_2$ thickness calibration curve in Figure 2(c). The maximum observed frequency difference between the peaks indicates a maximum possible thickness difference of less than 0.5 molecular layers, or about 3 Å. In conjunction with TEM results, it appears that the films are uniform to within one atomic diameter over the entire 4 $cm^2$ area. The relationship between processing conditions and this exceptional thickness uniformity is discussed in more detail later in this work.

Another hallmark of monolayer thin $MoS_2$ is photoluminescence (PL) due to the presence of a direct band gap at approximately 1.9 eV. Figure 3 shows the Raman shift as well as the PL from 3 and 5 layer $MoS_2$ samples grown on $SiO_2$. The PL spectra are relatively broad as they were taken at room temperature, but are similar to spectra reported by other authors.[7] This photoluminescence was observed for sputtered films with thicknesses up to 6 molecular layers.

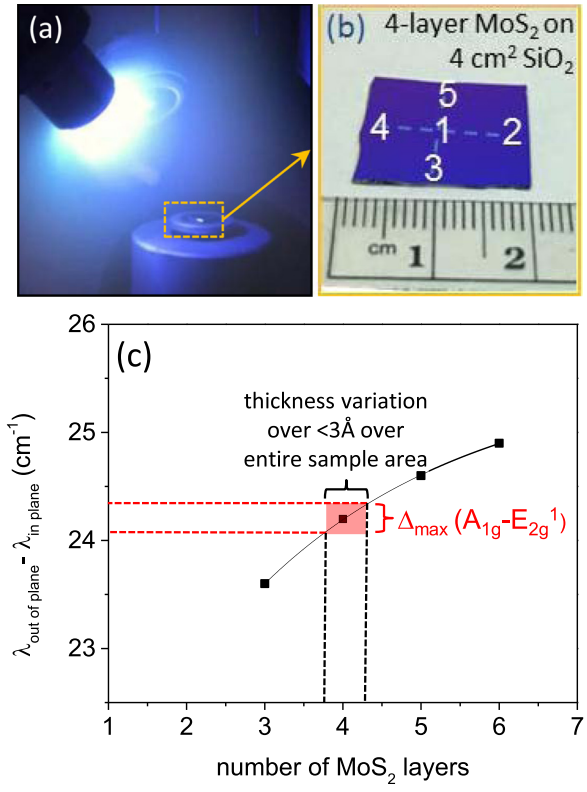


FIG. 2. (a) Photograph of 4 layer $MoS_2$ film growth process on a 2 cm × 2 cm wafer (b). The uniformity of the film was characterized with Raman spectroscopy at different locations on the sample surface as indicated in (b). Data from the numbered locations allowed calculation of a thickness difference of approximately 3 Å (c).

Very little to no PL intensity was observed for thicker films or bulk $MoS_2$ due to the decrease in the intraband relaxation rate from the excitonic states with decreasing film thickness, which thereby enhanced photoluminescence.[13] It was also verified that the measured PL intensity did not originate from the thermally oxidized ($SiO_2$/Si) substrate itself.

The $MoS_2$ films on $SiO_2$ show layer by layer growth without island formation in atomic force microscopy (Fig. 4(a)). Imaging of film surfaces was performed in peak-force quantitative nano-mechanical mapping mode. The high-resolution imaging was accomplished through use of a low setpoint (<20 mV) during sample engagement and throughout imaging, thereby preserving the tip shape. The RMS roughness of the film was approximately 0.58 nm compared to 0.26 of the substrate. This ultra-thin TMD film morphology can be attributed to the non-equilibrium sputtering process, where the incident atoms traverse sufficient distances upon arrival at the growing film surface to allow adsorption at high energy sites such as an atomic vacancy or step edge. The typical kinetic energies of incident atoms are on the order of 1–10 eV even after multiple scattering events within the background gas. This results in orders of magnitude greater energy input to the growing film surface as compared to the typical thermal energy associated with CVD growth, allowing increased surface mobility of incident atoms at relatively low substrate temperatures, such as the 350 °C employed here. For a growth process with high atomic surface mobility, it is generally recognized that layer by layer, or 2D growth occurs when $\gamma_f + \gamma_I < \gamma_s$, as the surface energy of the substrate ($\gamma_s$) will be reduced by coverage with the growing film, making such growth an energetically favorable process. For $MoS_2$ (with a surface energy of 260 erg $cm^{-2}$)[19] grown on low surface energy substrates such as $SiO_2$ (259 erg $cm^{-2}$),[20] the $\gamma_f$ and $\gamma_s$ values are approximately equivalent; therefore, the energy associated with creating the interface would act as a barrier for 2D growth. However, layer by layer growth still occurs as shown by the AFM and TEM results presented here. A monolayer of molybdenum may be the first layer grown on the surface, according to reports of the early studies of growth of van der Waals (vdW) materials via vapor phase growth.[21] This molybdenum layer would strongly bind to the oxide surface, as Mo has a large thermodynamic driving force to form an interfacial oxide *in situ* on an oxidized substrate.[22] It is hypothesized, that after the growth of the molybdenum monolayer, subsequent adsorption of incident sulfur and molybdenum atoms would result in edges with much higher surface energies (25 000 erg/$cm^{-2}$)[23] than the planar film surfaces parallel to the substrate surface. The high surface energy of anisotropic $MoS_2$ edges acting as 2D nuclei forming on this initial molybdenum base layer promotes 2D nucleation and growth, as incident atoms preferentially assemble at the reactive $MoS_2$ domain edges.

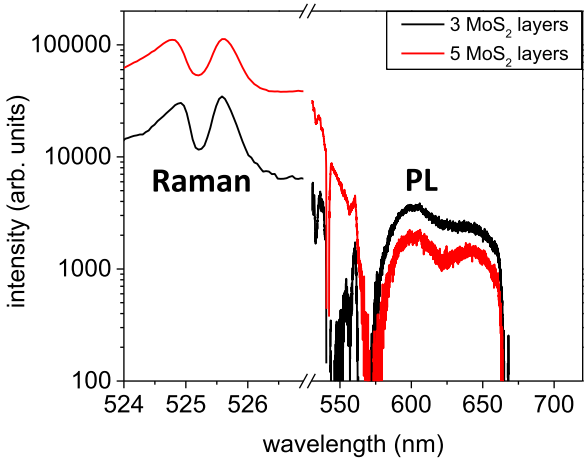


FIG. 3. Semi-log plot of Raman and PL for samples of 3 and 5 layer samples show how Raman intensity increases with the total $MoS_2$ volume sampled and PL quantum efficiency increases as material thickness is reduced.

Further support for hypothesized growth mechanisms is indicated by the morphology and composition of the $MoS_2$ films grown on HOPG substrates (Fig. 4(b)). While the lower surface energy of the HOPG (~80 erg $cm^{-2}$) should result in growth of isolated islands, a continuous network of granular topographic features was observed in the AFM in Figure 4(b) for the ~1.5 nm thick film. Coverage of the HOPG surface with a transition metal layer may temper the effects of the significantly lower substrate surface energy, resulting in a similar film morphology. An example of tri-layer $MoS_2$ grown on a HOPG surface is shown in Figure 4(c). HOPG and hexagonal $MoS_2$ have in-plane lattice mismatch of approximately 30%. Despite this extreme mismatch, the capability of growing well-oriented $MoS_2$ with the basal planes parallel to that of the HOPG was demonstrated. This result suggests that it is possible to grow van der Waals heterostructures[24] by PVD techniques, allowing selection of materials based on functionality with no regard for lattice matching.

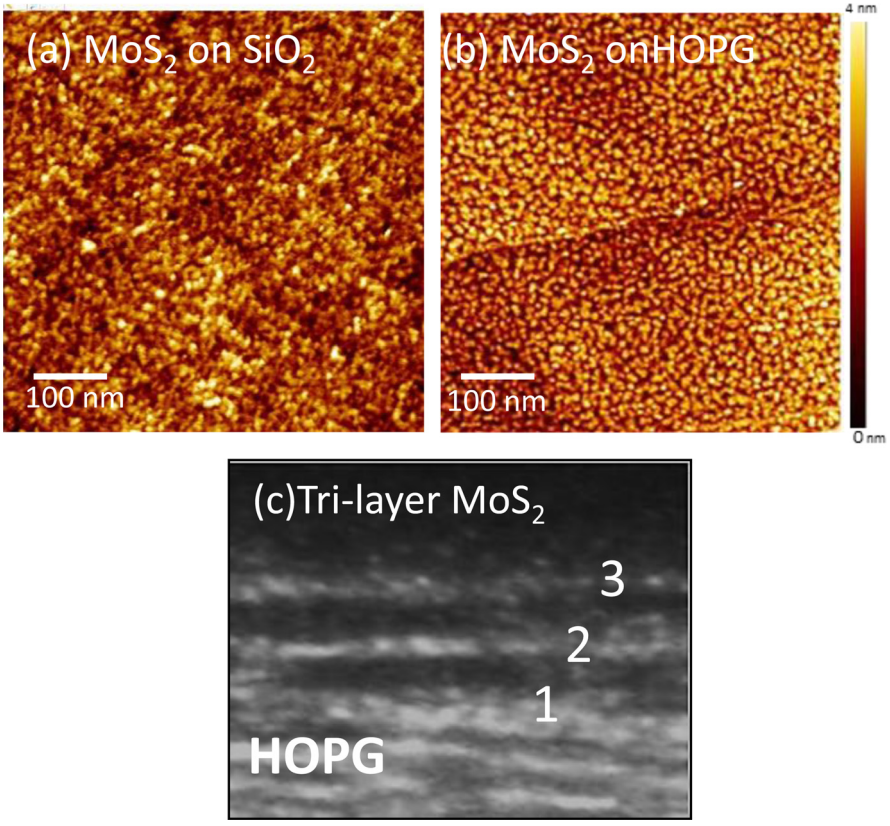


FIG. 4. AFM scans of 3 layer $MoS_2$ on (a) $SiO_2$ substrate and (b) HOPG substrate. A TEM cross-section of tri-layer $MoS_2$ on HOPG is shown in (c).

Film-substrate interface chemistry was examined with X-ray photoelectron spectroscopy (XPS) on these ultra-thin films, and the results support the proposed growth mechanisms for both substrates. It is presumed that Mo atoms, rather than sulfur comprise the first interfacial atomic layer, and hence, the evidence of this Mo-O interaction on the $SiO_2$ surface can be expected in the XPS analysis, since the $MoS_2$ overlayer is thin enough to allow escape of photoelectrons originating from the buried interfacial layer. Figure 5(a) shows that the total oxygen signal decreases with the increasing of $MoS_2$ thickness from 3 to 6 molecular layers. This is expected, as the probability of electrons escaping from the $SiO_2$ substrate decreases exponentially with increasing $MoS_2$ thickness. Evidence of the formation of Mo-O bonding at the $SiO_2$-$MoS_2$ interface comes from the examination of the high resolution scans of Mo 3 d peaks from the three- and six-layer films (Fig. 5(b)). Curve fitting of the high-resolution XPS data reveals that the Mo $3d_{3/2}$ peak from $MoO_3$ (235.7 eV) decreases in intensity relative to the Mo $3d_{5/2}$ peak from $MoS_2$ (229.0 eV) as the overlayer thickness increases from three to six layers. This peak at 235.7 eV is indicative of $MoO_3$ formation rather than substituional oxygen incorporated into the film during synthesis.[25] This suggests that the Mo-O bonds originate from the interface region (rather than from within $MoS_2$), indicating that the initial adlayer consists of Mo atoms bound to the O atoms of the substrate, while further deposition results in a $MoS_2$ film with a lower oxygen content. Moreover, the S 2s peak (226.4 eV) increases in intensity relative to the Mo $3d_{3/2}$ peak from $MoO_3$ as the film thickness increases, further supporting the model of a Mo-O interfacial layer buried by an $MoS_2$ overlayer.

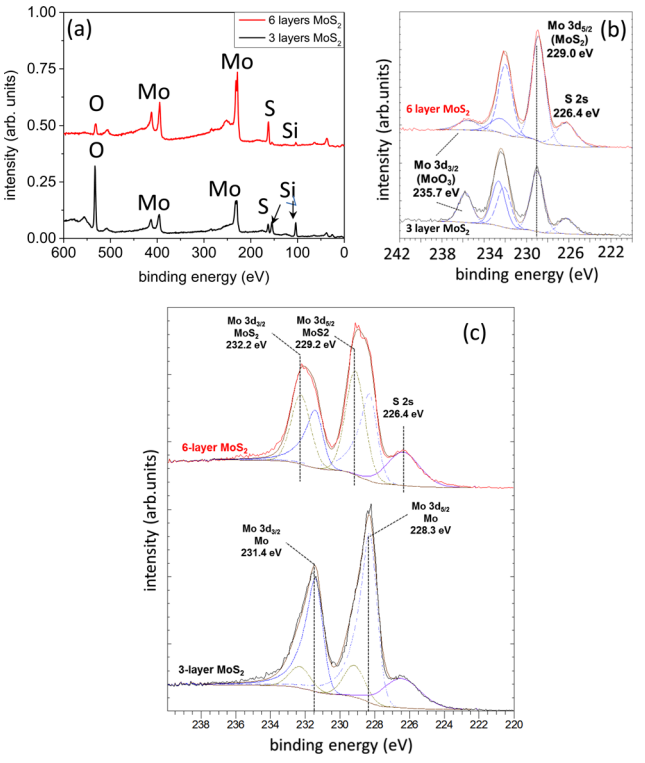


FIG. 5. X-ray photoelectron spectroscopy data for $MoS_2$ samples on $SiO_2$. The survey scans for 3 and 6 layer thick $MoS_2$ films (a) reveal higher silicon and oxygen peaks from the substrate due to the increased electron transparency of the thinner sample. A high resolution scan of the Mo (3d) peaks (b) reveal a diminished $MoO_3$ signal as the interface is buried deeper under the film and the electron transparency is reduced. For $MoS_2$ films grown on HOPG (c), the $MoO_3$ peak is absent and the Mo 3d5/2 peaks show strong metallic character for 3 layer films, with a much stronger Mo-S contribution for thicker films.

For film thicknesses beyond the interfacial Mo layer, XPS data provide critical validation of $MoS_2$ compound formation in Fig. 5(b). Here, X-ray photoelectron spectroscopy shows a single Mo $3d_{5/2}$ peak at to 229.0 eV (Mo IV), which is a clear indicator of covalent Mo-S bonding comprising the metal dichalcogenide, as a mixture with metallic Mo would give rise to two distinct peaks.[26] While analysis shows compound formation, the precise composition of the films was not directly quantified with XPS due to challenges associated with ambient contamination on molecularly thin films. It is anticipated that they may be slightly sulfur deficient, as most sputtered $MoS_2$ films are due to interactions with incident hydrogen or oxygen ions or atoms from ambient water that is present even within the vacuum environment employed in the current work.

Three and six layer $MoS_2$ films grown on HOPG were also examined with XPS (Fig. 5(c)), to demonstrate that there is no $MoO_3$ formation (at the interface or elsewhere) and that the nature of the Mo bonds changes from metallic Mo-Mo (distinctly characterized by an asymmetric peak at 228 eV) to Mo-S as film thickness increases. The existence of the 1T $MoS_2$ phase rather than the 2H phase could also give rise to this peak at 228 eV; however, annealing of the samples to 200 °C did not remove this component. High resolution sulfur peaks were also analyzed, and did not show the 1T characteristics.[3] As for the $MoS_2$ films grown on $SiO_2$, the presence of metallic Mo decreased with increasing thickness, suggesting the presence of an interfacial Mo layer at the HOPG/$MoS_2$ film interface.

In summary, a scalable approach for uniform growth of continuous 2D TMD films on substrates >4 $cm^2$ was demonstrated. The PVD process allows a growth of $MoS_2$ at lower temperatures (350 °C in this work) directly on thermally grown silicon oxide and (002) graphite. The growth process is based on sputtering and is easily applicable to other transition metal dichalcogenides. The materials demonstrate the properties of exfoliated materials. Experiments with the PVD growth on diverse substrates including sapphire, borosilicate glass, and polycrystalline metals are ongoing with similar results, which will be discussed in future work. Low temperature PVD synthesis of 2D TMD materials provides a desirable combination of uniformity and scalability.

C.M. gratefully acknowledges Advanced Energy Industries Inc. for use of the Pinnacle Plus pulsed power supply for all synthesis in this work. All authors acknowledge Mr. Art Safriet for support with modifications of the growth chamber required to perform this work.

[1]W. E. Jamison and S. L. Cosgrove, ASLE Trans. **14**, 62 (1971).
[2]R. R. Chianelli, M. H. Siadati, M. P. de la Rosa, G. Berhault, J. P. Wilcoxon, R. Beardon, and B. L. Abrams, Catal. Rev.: Sci. Eng. **48**, 1 (2006).
[3]G. Eda, H. Yamaguchi, D. Voiry, T. Fujita, M. Chen, and M. Chhowalla, Nano Lett. **11**, 5111 (2011).
[4]J. Feng, X. Qian, C.-W. Huang, and J. Li, Nat. Photonics **6**, 866 (2012); K. He, C. Poole, K. F. Mak, and J. Shan, Nano Lett. **13**, 2931 (2013); Y. Y. Hui, X. Liu, W. Jie, N. Y. Chan, J. Hao, Y.-T. Hsu, L.-J. Li, W. Guo, and S. P. Lau, ACS Nano **7**, 7126 (2013); H. Peelaers and C. G. Van de Walle, Phys. Rev. B **86**, 241401 (2012).
[5]K. F. Mak, C. Lee, J. Hone, J. Shan, and T. F. Heinz, Phys. Rev. Lett. **105**, 136805 (2010).
[6]H. Terrones, F. Lopez-Urias, and M. Terrones, Sci. Rep. **3**(203), 1549 (2013).
[7]H. Li, Q. Zhang, C. C. R. Yap, B. K. Tay, T. H. T. Edwin, A. Olivier, and D. Baillargeat, Adv. Funct. Mater. **22**, 1385 (2012).
[8]H. Li, Z. Yin, Q. He, H. Li, X. Huang, G. Lu, D. W. H. Fam, A. I. Y. Tok, Q. Zhang, and H. Zhang, small **8**, 63 (2012).
[9]F. K. Perkins, A. L. Friedman, E. Cobas, P. M. Campbell, G. G. Jernigan, and B. T. Jonker, Nano Lett. **13**, 668 (2013).
[10]Q. H. Wang, K. Kalantar-Zadeh, A. Kis, J. N. Coleman, and M. S. Strano, Nat. Nanotech. **7**, 699 (2012).
[11]M. R. Laskar, L. Ma, S. Kannappan, P. S. Park, S. Krishnamoorthy, D. N. Nath, W. Lu, Y. Wu, and S. Rajan, Appl. Phys. Lett. **102**, 252108 (2013); Y. Lee, J. Lee, H. Bark, I.-K. Oh, G. H. Ryu, Z. Lee, H. Kim, J. H. Cho, J.-H. Ahn, and C. Lee, Nanoscale **6**, 2821 (2014); Y.-H. Lee, X.-Q. Zhang, W. Zhang, M.-T. Chang, C.-T. Lin, K.-D. Chang, Y.-C. Yu, J. T.-W. Wang, and C.-S. Chang, Adv. Mater. **24**, 2320 (2012); X. Ling, Y.-H. Lee, Y. Lin, W. Fang, L. Yu, M. S. Dresselhaus, and J. Kong, Nano Lett. **14**, 464 (2014); S. Najmaei, Z. Liu, W. Zhou, X. Zou, G. Shi, S. Lei, B. I. Yakobson, J.-C. Idrobo, P. M. Ajayan, and J. Lou, Nat. Mater. **12**, 754 (2013); A. M. van der Zande, P. Y. Huang, D. A. Chenet, T. C. Berkelbach, Y. You, G.-H. Lee, T. F. Heinz, D. R. Reichman, D. A. Mueller, and J. C. Hone, Nat. Mater. **12**, 554 (2013).
[12]H.-P. Komsa, S. Kurasch, O. Lehtinen, U. Kaiser, and A. V. Krasheninnikov, Phys. Rev. B **88**, 035301 (2013).
[13]A. Splendiani, L. Sun, Y. Zhang, T. Li, J. Kim, C.-Y. Chim, G. Galli, and F. Wang, Nano Lett. **10**, 1271 (2010).
[14]C. Muratore, V. Varshney, J. J. Gengler, J. Hu, J. E. Bultman, A. K. Roy, B. L. Farmer, and A. A. Voevodin, Phys. Chem. Chem. Phys. **16**, 1008 (2014); C. Muratore and A. A. Voevodin, Thin Solid Films **517**, 5605 (2009).
[15]C. Muratore and A. A. Voevodin, Ann. Rev. Mat. Sci. **39**, 297 (2009).
[16]C. Muratore, V. Varsheny, J. J. Gengler, J. J. Hu, J. E. Bultman, T. M. Smith, P. J. Shamberger, B. Qiu, X. Ruan, A. K. Roy, and A. A. Voevodin, Appl. Phys. Lett **102**, 081604 (2013).
[17]C. Lee, H. Yan, L. E. Brus, T. F. Heinz, J. Hone, and S. Ryu, ACS Nano **4**, 2695 (2010).
[18]Y. Zhan, Z. Liu, S. Najmaei, P. M. Ajayan, and J. Lou, Small **8**, 966 (2012).
[19]K. Weiss and J. M. Phillips, Phys. Rev. B **14**, 5392 (1976).
[20]S. Brunauer, D. L. Kantro, and C. H. Weise, Can. J. Chem. **34**, 1483 (1956).
[21]A. Koma, K. Sunouchi, and T. Miyajima, Microelectron. Eng. **2**, 129 (1984); F. S. Ohuchi, T. Shimada, B. A. Parkinson, K. Ueno, and A. Koma, J. Cryst. Growth **111**, 1033 (1991).
[22]B. N. Chapman, J. Vac. Sci. Technol. **11**, 106 (1974).
[23]J. A. Spirko, M. L. Neiman, A. M. Oelker, and K. Klier, Surf. Sci. **542**, 192 (2003).
[24]A. K. Geim and I. V. Grigorieva, Nature **499**, 419 (2013).
[25]P. D. Fleischauer and J. R. Lince, Tribol. Int. **32**, 627 (1999); J. R. Lince, M. R. Hilton, and A. S. Bommannavar, Surf. Coat. Technol. **43/44**, 640 (1990).
[26]J. R. Lince, D. J. Carre, and P. D. Fleischauer, Langmuir **2**, 805 (1986).